31st Annual International Conference of the IEEE EMBS
Minneapolis, Minnesota, USA, September 2-6, 2009

Modeling and Optimization of Printed Spiral Coils in Air and Muscle Tissue Environments

Uei-Ming Jow, *Student Member, IEEE*, and Maysam Ghovanloo, *Member, IEEE*

***Abstract*—Printed spiral coils (PSC) are viable candidates for near field wireless power transmission to the next generation of prosthetic devices with extreme size constraints. Implantable devices need to be hermetically sealed in biocompatible materials and placed in conductive environment with high permittivity, which can affect the PSC characteristics. We have constructed a detailed model that includes the effects of surrounding environment on the PSC parasitic components and eventually on the power transfer efficiency. This model is combined with an iterative design method that starts with a set of realistic design constraints and ends with the optimal PSC geometries. This was applied to optimize the wireless link of a 1 cm^2 implantable device operating at 13.56 MHz. Measurement results showed that optimized PSC pairs, coated with 0.3 mm of silicone, achieved 72.2% and 30.8% efficiencies at a face to face relative distance of 10 mm in the air and muscle environment respectively. The PSC which was optimized for air could only bear 21.8% efficiency in muscle, showing that considering the PSC surrounding environment in the design process can result in nearly 10% improvement in the power transfer efficiency.**

I. Introduction

COCLHEAR implants, spinal cord stimulators, infusion pumps, and artificial hearts are among an ever-growing group of implantable devices that are wirelessly powered across the skin through a pair of inductively coupled coils [1]. A common requirement among these otherwise diverse biomedical devices is that their average power consumption is higher than what a battery, fitting within the anatomically available space for implantation, can provide. Therefore, the need for more efficient wireless power transmission from outside into the human body is only expected to grow. This would require microfabrication techniques that result in lithographically defined planar structures known as printed spiral coils (PSC). We recently studied simple models of PSC in [2] and combined the theoretical foundation of optimal power transmission with these simple models. The result was an iterative PSC design methodology for maximum power efficiency [2]. However, implantable devices are hermetically sealed in biocompatible materials and surrounded by the conductive tissue underneath the skin. Considering the effects of surroundings in PSC models is imperative in the optimization process because of parasitic components, which in turn affect the power transfer efficiency.

This work was supported in part by the National Institute of Health grant 1R01NS062031-01A1, and the National Science Foundation under award ECCS-824199.

Uei-Ming Jow and Maysam Ghovanloo* are with the GT-Bionics lab (www.GTBionics.org), School of Electrical and Computer Engineering at the Georgia Institute of Technology, Atlanta, GA 30308, USA (phone: 404-385-7048; fax: 404-894-4701, email: mgh@gatech.edu).

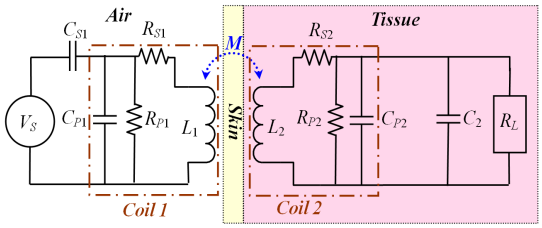

Fig. 1. Simplified schematic diagram of the inductive link with lumped equivalent circuit components.

Fig. 1 shows a simplified schematic diagram of a transcutaneous inductive power transmission link with parasitic components. L_1 is the primary coil that is attached to the skin from outside, driven by an amplifier, V_S, and L_2 is the secondary coil implanted under the skin with the implant electronics. M is the mutual inductance between L_1 and L_2. Coil windings have parasitic resistance and capacitance associated with them, which are represented by lumped elements R_S, R_P, and C_P. Capacitors, C_{S1} and C_2, are also added to form a pair of resonant LC-tank circuits with L_1 and L_2, respectively, at the power carrier frequency, f.

In this paper, we improve the accuracy of our PSC model in section II by adding the effects of the coating, substrate, and surrounding environments. We also consider some of the key secondary effects in estimating parasitic components for PSC quality factors, Q. In section III, we utilize the new models in the same iterative optimization method as in [2], using a combination of closed form equations in MATLAB and verification with finite element analysis (FEA) tools in HFSS (Ansoft, Pittsburgh, PA). The result is two sets of PSCs, which geometries are optimized for air and muscle environments. These PSCs were fabricated on FR4 and characterized in both environments in section IV to compare their power transfer efficiency, and validate our PSC models and iterative design procedure.

II. Theoretical Modeling of Implanted PSCs

In the following, we construct a realistic theoretical model for PSCs. The lumped parasitic components of the PSC model are influenced by its geometry, material composition, and surrounding environment.

A. Inductance

In this work, all PSCs are square shaped with rounded corners that have a radius of about a tenth of the side length of the PSC (d_o/10) to eliminate sharp edges. We adopted (1) from [3] for calculating the inductance of square shaped coils,

$$L = \frac{1.27 \cdot \mu n^2 d_{avg}}{2}\left[\ln\left(\frac{2.07}{\varphi}\right) + 0.18\varphi + 0.13\varphi^2\right], \qquad (1)$$

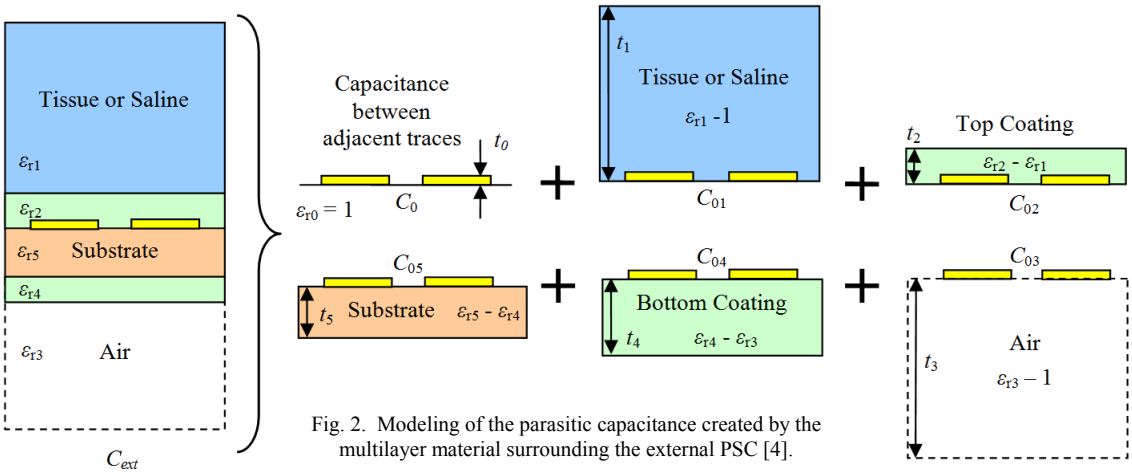

Fig. 2. Modeling of the parasitic capacitance created by the multilayer material surrounding the external PSC [4].

where n is the number of turns, μ is permeability, and $d_{avg} = (d_o + d_i)/2$, where d_o and d_i are the outer and inner side lengths of the coil, respectively. $\varphi = (d_o - d_i)/(d_o + d_i)$ is a parameter known as fill factor. The accuracy of (1) has an indirect relationship with the s/w ratio, where w and s are the PSC metal line width and spacing, respectively. According to [3], the error in (1) is 8% for $s/w = 3$ and increases for $s/w > 3$. Moreover, the accuracy of (1) degrades with $\varphi \le 0.1$ or $n \le 2$.

B. Capacitance

In its realistic form, the implanted coil will be surrounded by tissue and fluids that have high permittivity, which increase the parasitic capacitance, C_P. Therefore, we consider the PSC traces as coplanar striplines to model the unit length parasitic capacitance, as shown in Fig. 2, which shows the cross section of two traces of the external PSC. One side of the PSC is air and the other side is the tissue. From conformal mapping [4] technique and superposition of individual layers, the total capacitance per unit length can be expressed as

$$C_{ext} = \varepsilon_{r-eff} C_0 = C_0 + C_{01} + C_{02} + C_{03} + C_{04} + C_{05}, \quad (2)$$

where $\varepsilon_{r\text{-}eff}$ is the effective relative dielectric constant of the multilayer structure, C_0 is the capacitance between adjacent traces in free space and C_{0i} (i = 1 to 5) is the additional partial capacitance of each planar dielectric layer. Theoretically,

$$C_0 = \varepsilon_0 \frac{K(k_0')}{K(k_0)},\ k_0 = \frac{2s}{s+2w},\ \text{and}\ k_0' = \sqrt{1-k_0^2}, \quad (3)$$

where $K(k_0)$ is the complete elliptic integral of the first kind.

$$\varepsilon_{r-eff} = 1 + \frac{1}{2}(\varepsilon_{r1} - 1)\frac{K(k_0)K(k'_1)}{K(k_0')K(k_1)} + \quad (4)$$
$$+ \frac{1}{2}(\varepsilon_{r2} - \varepsilon_{r1})\frac{K(k_0)K(k'_2)}{K(k_0')K(k_2)} + \frac{1}{2}(\varepsilon_{r3} - 1)\frac{K(k_0)K(k'_3)}{K(k_0')K(k_3)}$$
$$+ \frac{1}{2}(\varepsilon_{r4} - \varepsilon_{r3})\frac{K(k_0)K(k'_4)}{K(k_0')K(k_4)} + \frac{1}{2}(\varepsilon_{r5} - \varepsilon_{r4})\frac{K(k_0)K(k'_5)}{K(k_0')K(k_5)}$$

$$k_i = \frac{\tanh(\pi s/4t_i)}{\tanh(\pi(s+2w)/4t_i)},\ k_i' = \sqrt{1-k_i^2},$$

where ε_{ri} and t_i are the relative dielectric constant and thickness of dielectric layers in Fig. 2, respectively [4].

Furthermore, a conductor should bridge across all other turns of the PSC in a different layer through a via to access the PSC inner terminal. Hence, an additional parasitic capacitance, C_{ov}, a parallel-plate capacitor between the two overlapping metal layers, should be included in C_P. Overall, the total parasitic capacitance of the external PSC can be

$$C_P = C_{ext} \cdot l_c + C_{ov}, \quad (5)$$

where l_c is the PSC conductor length.

For the implanted PSC, we can utilize (2) to (5) with the exception that the dielectric layer 3 (air) should be replaced by the tissue properties, similar to layer 1, depending on the anatomical location of the implanted device.

C. Series Resistance

The series resistance, R_S, is dominated by the two effects. The first effect is the skin effect, and the related resistance is

$$R_{skin} = \rho_c \frac{l_c}{w \cdot t_0} \cdot \frac{t_0}{\delta \cdot (1 - e^{-t_0/\delta_{skin}})} \cdot \frac{1}{1 + t_0/w}, \quad (6)$$

where ρ_c is the resistivity of conductive material and δ_{skin} is the skin depth [5]. Another effect is the current crowding caused by the eddy currents, modifying the resistance as,

$$R_{eddy} = \frac{1}{10}\rho_c \frac{l_c}{w \cdot t_0}\left(\omega \Big/ \frac{3.1}{\mu_0}\frac{s+w}{w^2} R_{sheet}\right)^2, \quad (7)$$

where R_{sheet} is the metal trace sheet resistance [6]. Therefore, R_S should be modified by the skin and eddy current effects as

$$R_S = R_{skin} + R_{eddy}. \quad (8)$$

D. Parallel Resistance

Dielectric losses, which are related to loss tangent, $tan(\delta)$, of each material, can affect the parallel resistance, R_P. In this case, we use the partial conductance technique combined with the conformal mapping. The conformal transformations required for the evaluation of partial conductivities due to different layers are similar to the partial capacitances described in section II.B [7]. For the external PSC, shown in Fig. 2, the equivalent conductance, G_P, of unit length is

$$\frac{1}{R_P} = G_P = \frac{\omega\varepsilon_0}{2}\left[\varepsilon_{r1}\tan\delta_1 \frac{K(k_1')}{K(k_1)} + (\varepsilon_{r2}\tan\delta_2 - \varepsilon_{r1}\tan\delta_1)\frac{K(k_2')}{K(k_2)}\right.$$
$$\left. + \varepsilon_{r3}\tan\delta_3 \frac{K(k_3')}{K(k_3)} + (\varepsilon_{r4}\tan\delta_4 - \varepsilon_{r3}\tan\delta_3)\frac{K(k_4')}{K(k_4)}\right.$$

TABLE I
MATERIAL PROPERTIES AT 13.56 MHZ [9]

Material	Air	Muscle	FR4	Silicone	PE
σ [S/m]	0	0.58	1.33e-4	2.26e-6	5.52e-8
ε_r	1	136	4.4	3.0	2.3
tan(δ)	0	6.0	0.04	0.001	0.0002

$$+(\varepsilon_{r5}\tan\delta_5-\varepsilon_{r4}\tan\delta_4)\frac{K(k_5')}{K(k_5)}\Bigg]. \quad (9)$$

The same equation can be used for equivalent conductance of the internal PSC.

E. Power Transfer Efficiency

From (1) to (9), we can derive all the parameters needed for calculating the overall impedance Z and the quality factor of the implanted and external PSCs, Q = Im (Z) / Re (Z). Moreover, the secondary PSC is often loaded by the implant electronics, R_L (Fig. 1), and according to [8], the loaded secondary quality factor can be found from

$$Q_L=\left(\frac{R_{S2}}{\omega L_2}+\frac{\omega L_2}{R_L \,||\, R_{P2}}\right)^{-1}. \quad (10)$$

On the other hand, the mutual inductance, M, can be found from [2]. Using M, we can find the coupling coefficient, $k = M/\sqrt{(L_1L_2)}$, which is the key parameter in power efficiency.

Regarding the power carrier frequency, the highest voltage gain and efficiency across an inductive link can be achieved when both LC-tanks are tuned at carrier frequency,

$$\omega=\omega_0=1/\sqrt{L_1C_{S1}}=1/\sqrt{L_2(C_2+C_{P2})}. \quad (11)$$

Therefore, the inductive link power transfer efficiency can be calculated from PSCs' k and quality factors [2],

$$\eta_{12}=\frac{k^2Q_1Q_L}{1+k^2Q_1Q_L}\cdot\frac{Q_L}{Q_2+Q_L}. \quad (12)$$

Note that another parameter is the V_S output resistance, not shown Fig. 1, which is out of the scope of this paper and needs to be considered with the driver's efficiency.

III. OPTIMIZATION OF PRINTED SPIRAL COIL

In this section, we use detailed models built in section II to design two sets of coils optimized for air and muscle tissue environments. The material properties of these volume conductors at f = 13.56 MHz, which is the power carrier frequency, are summarized in Table I [9]. The size of the implant is 10×10 mm^2 [1]. The nominal coupling distance is considered d = 10 mm. We have adopted the iterative design procedure, described in [2], and HFSS simulations are also utilized to verify and fine tune the values suggested by the theoretical model, when they were out of the valid range of our equations (ex. PSC21). Table II shows the geometries of the resulting PSCs, specifically optimized for each environment, when the PSC pair is perfectly aligned.

Another important design parameter is the thickness of the coating. Fortunately, the dielectric constant, ε_r, of silicone coating is much lower than any type of human tissue (Table I). Therefore, increasing the thickness of the coating will reduce C_P and increase R_P, both of which help increasing Q and consequently η_{12}. On the other hand, increasing the thickness of the coating will increase d and the volume of the implant. Nevertheless, we found it instructive to indicate the optimal coating thickness, t_2 = ~300 μm, by sweeping t_2 in our model (Fig. 2), while maintaining all other parameters constant.

TABLE II
OPTIMIZED PSC GEOMETRIES AND INDUCTIVE LINK CHARACTERISTICS FROM SIMULATION RESULTS*

Parameter	Set-1		Set-2	
Material	**Air**		**Muscle**	
Name	PSC11	PSC12	PSC21	PSC22
d_o (mm)	38	10	24	10
n (turns)	7	6	2	4
w (μm)	1500	200	3500	150
s (μm)	150	150	150	150
L (μH)	1.66	0.51	0.12	0.34
R_S (Ω)	0.93	0.72	0.06	0.72
R_P (kΩ)	758	3120	2.36	1.68
C_P (pF)	3.12	0.18	7.72	0.77
C_{s1} / C_2 (pF)	83.0	270.1	1148	450
Q	128	60	96	32
k	0.0697		0.0301	
η_{12_cal} (%)♦	72.05		29.85	
η_{12_sim} (%)	74.86		27.70	
η_{12_meas} (%)♠	72.22		30.84	

*For perfectly aligned PSCs with a nominal coupling distance of d = 10 mm at f = 13.56 MHz and R_L = 500 Ω, coated with a 300 μm layer of silicone.
♦Calculation results. ♠Measurement results.

IV. SIMULATION AND MEASUREMENT RESULTS

We used a network analyzer (R&S ZVB4) to measure the S-parameters, which were converted to Z-parameters to calculate k and Q to find η_{12}. In addition to measurements in air, we used two plastic bags made by polyethylene (PE) (~50 μm thick), and filled them with beef (sirloin steak at 10.8 °C) to emulate the environments around an implanted device. The internal PSC was sandwiched between the two bags while the external PSC was aligned with it, touching the outer surface of one of the bags. The beef thickness behind the internal PSCs, t_3, was 50 mm.

A. PSC Quality Factor

Fig. 3 shows how the Q of coated PSC11 and PSC21 change vs. frequency in the air and muscle environments. At13.56 MHz, Q of PSC11 decreases by 78% in the muscle environment due to changes in C_P and R_P. On the other hand, Q of PSC21 decreases only by 25% in muscle. The agreement among calculation, simulation, and measurement results in Fig. 3 clearly demonstrate the efficacy of the geometrical optimization algorithm and models described in section II.

B. Power Transfer Efficiency

In Figs. 4a and 4b, we have compared the power transfer efficiency of the PSCs in Table II in the air and muscle environments, respectively, through model-based theoretical calculations, FEA-based simulations, and experimental measurements. PSCs are perfectly aligned and their coupling distance on the horizontal axis includes their coating thickness (300 μm). The secondary PSC is loaded with R_L = 500 Ω. Fig. 4 curves show that each set of PSCs performs

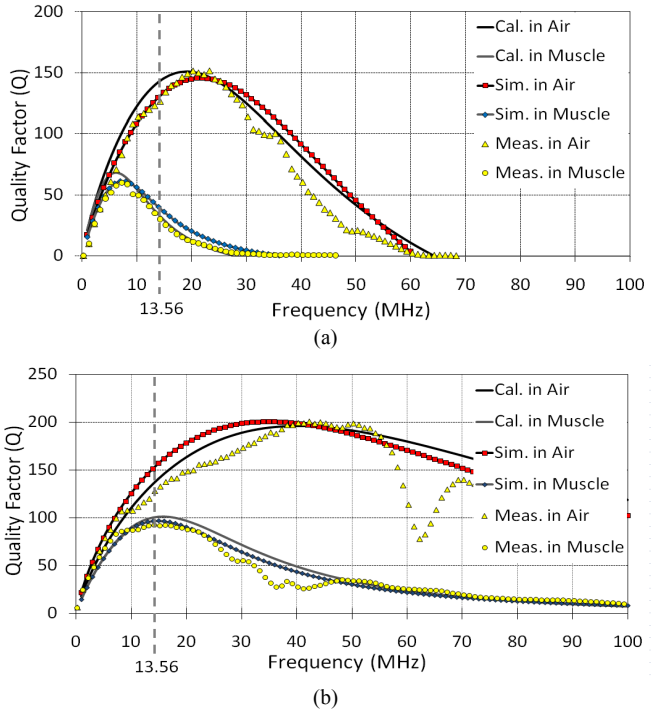

Fig. 3. Comparison between theoretical calculations, HFSS simulations, and measurement results of Q variations vs. carrier frequency in (a) PSC11 that is optimized for air, and (b) PSC21 that is optimized for muscle. (Table II).

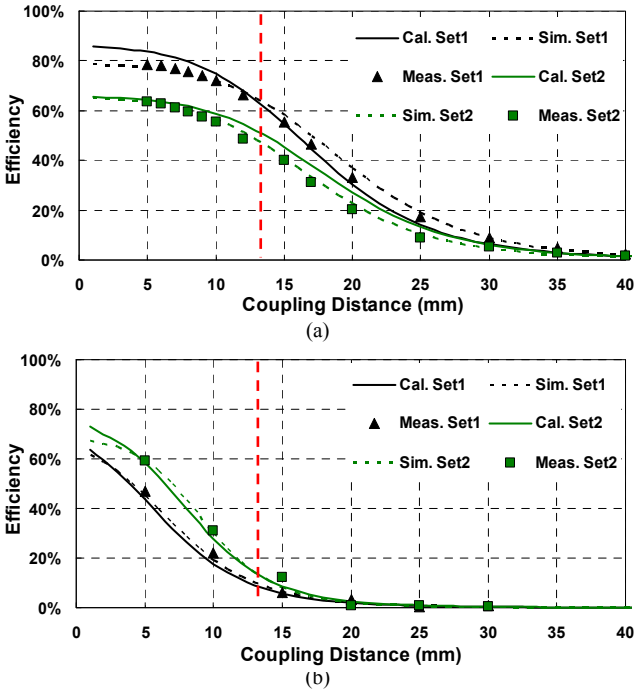

Fig. 4. Variations of the power transfer efficiency with coupling distance at 13.56 MHz for three sets of PSCs in Table II optimized for (a) air and (b) muscle environments.

best in its designated operating environment. Fig. 4b obviously shows that a pair of PSCs that is optimized for air (Set-1) provides worse η_{12} when implanted in the muscular tissue. While Set-1 PSC pair can achieve more than 70% efficiency in the air due to their high k, its η_{12} drops to only 21.8% in the muscle environment due to degradation in their Q, as seen in Fig. 3a. Set-2 pair, on the other hand, provides $\eta_{12} > 30\%$ at $d = 10$ mm due to PSC21 smaller geometries, which is optimized for this environment.

Fig. 4 also shows reasonable agreement among theoretical calculations from our models, finite element simulations, and measurement results. There are, however, small discrepancies due to the following reasons, some of which are related to our models and the measurement setup: 1) inherent limitations in the accuracy of the closed form equations, particularly when the PSC parameters are close to or out of their valid range of parameters, 2) secondary effects such fringing and capacitive coupling between PSCs, which were not included in our models, 3) manually applied silicone coating was not quite uniformly distributed on the PSC surfaces, 4) there could be small patches of air gap between the plastic bags containing the volume conductors and the outer surface of the PSCs' silicone coating, and 5) Thickness of the plastic bag (50 μm), which was considered to be part of the PSC silicone coating.

V. Conclusions

Various phenomena that could result in degradation of the PSC quality factors due to coating and implantation are considered in new our models. We combined our models with an iterative PSC design procedure, described in [2], to optimize the PSC geometries for maximum power transfer efficiency in tissue environments. This can result in lower heat dissipation [11], extended battery lifetime, and improved safety in neuroprosthetic devices, such as retinal or cortical implants, with demanding size constraints.

References

[1] M.S. Humayun *et al.*, "Visual perception in a blind subject with a chronic microelectronic retinal prosthesis," *Vision Research*, vol. 43, pp. 2573-2581, Nov. 2003.

[2] U. Jow and M. Ghovanloo, "Design and optimization of printed spiral coils for efficient transcutaneous inductive power transmission," *IEEE Trans. Biomed. Cir. Sys.*, vol. 1, no. 3, pp. 193-202, Sep. 2007.

[3] S.S. Mohan, M. del Mar Hershenson, S.P. Boyd, and T.H. Lee, "Simple accurate expressions for planar spiral inductances," *IEEE J. Solid-State Circuits*, vol. 34, no. 10, pp. 1419-1424, Oct. 1999.

[4] P. Pieters, K. Vaesen, S. Brebels, S.F. Mahmoud, W. DeRaedt, E. Beyne, and R.P. Mertens, "Accurate modeling of high-Q spiral inductors in thin-film multilayer technology for wireless telecommunication applications," *IEEE Trans. Microwave Theory Tech.,* vol. 49, no. 4, pp. 589-599, Apr. 2001.

[5] H.A. Wheeler, "Formulas for the skin effect," *Proceedings of the IRE,* vol. 30, no. 9, pp.412-424, Sep. 1942.

[6] W.B. Kuhn and N.M. Ibrahim, "Analysis of current crowding effects in multiturn spiral inductors," *IEEE Trans. Microwave Theory Tech.,* vol. 49, no. 1, pp. 31-38, Jan. 2001.

[7] S. Gevorgian, H. Berg, H. Jacobsson and T. Lewin, "Basic parameters of coplanar-strip waveguides on multilayer dielectric/semiconductor substrates, Part 1: high permittivity superstrates," *IEEE Microwave Magazine*, vol. 4, no. 2, pp. 60-70, June 2003.

[8] K. Finkenzeller, *RFID Handbook: Fundamentals and Applications in Contactless Smart Cards and Identification*, 2nd ed., Hoboken, NJ: John Wiley & Sons, 2003.

[9] C.M. Zierhofer, and E.S. Hochmair, "Geometric approach for coupling enhancement of magnetically coupled coils," *IEEE Trans. Biomedical Engineering,* vol. 43, no. 7, pp.708-714, July 1996.

[10] S. Gabriel, R.W. Lau, and C. Gabriel, "The dielectric properties of biological tissues: II. Measurements in the frequency range 10 Hz to 20 GHz," *Phys. Med. Biol.*, vol. 41, pp. 2251-2269, Nov. 1996.

[11] G. Lazzi, "Thermal effects of bioimplants," *IEEE Eng. in Med. Biol. Magazine*, vol. 24, no. 5, pp. 75-81, Sep. 2005.